In Situ FT-IR Study on the Homogeneous Nucleation of Nanoparticles of Titanium Oxides from Highly Supersaturated Vapor

Shinnosuke Ishizuka, Yuki Kimura[*]*, and Tomoya Yamazaki*

Institute of Low Temperature Science, Hokkaido University, Kita-19, Nishi-8, Kita-ku, Sapporo 060-0819, Japan.

[*]Corresponding Auther. TEL: +81-11-706-7666

E-mail adress: ykimura@lowtem.hokudai.ac.jp (Yuki Kimura)

Abstract

The formation of nanoparticles of titanium oxides by homogeneous nucleation from highly supersaturated vapors was investigated by in situ Fourier transform IR spectroscopy and by observation of the resulting nanoparticles by transmission electron microscopy (TEM). Titanium metal was thermally evaporated in a specially designed chamber under a gaseous atmosphere of oxygen and argon. Nanoparticles nucleated and subsequently grew as they flew freely through the oxidizing gas atmosphere. Nascent nanoparticles of titanium oxides showed a broad IR absorption band at 10–20 μm. Subsequently, the cooled nanoparticles showed a sharp crystalline anatase feature at 12.8 μm. TEM observations showed the formation of spherical anatase nanoparticles. The IR spectral evolution showed that the titanium oxides nucleated as metastable liquid droplets, and that crystallization proceeded through secondary nucleation from the supercooled liquid droplets. This suggests that history of the titanium oxide nanoparticles, such as the temperature and oxidation that they experience after nucleation, determines their polymorphic form.

Keywords

A1. Nucleation, A3. Physical vapor deposition process B1. Nanomaterials, B1. Oxides

1. Introduction

The TiO_2 system contains three naturally occurring polymorphs: rutile, anatase, and brookite. The synthesis of nanocrystalline titanium oxides by homogeneous nucleation from the vapor phase often results in the formation of anatase, which is known to be a metastable phase in the bulk oxide.[1–3]

Thermodynamic stability at the nanoscale is strongly influenced by surface energetics. Some oxides have several polymorphs such as alumina,[4,5] hafnia,[6] zirconia,[7–9] and titania[10,11], which show size-dependent crossovers of phase stability. Although rutile is known to be the stable phase in bulk TiO_2 under ambient conditions, theoretical studies have suggested that anatase becomes the stable phase when particle size is less than 15 nm in vacuum, because of the lower average surface free energy of anatase (1.32 $J \cdot m^{-2}$) compared with rutile (1.91 $J \cdot m^{-2}$).[12] Furthermore, according to calculations based on density functional theory, amorphous TiO_2 is thermodynamically stable when its nanoparticles are smaller than about 2 nm.[13] In contradiction to the thermodynamic stability, the appearance of anatase at sizes above the stability limit is often observed. Formation of the metastable anatase particles has been proposed as a result of subsequent growth of anatase nuclei without phase transition to stable rutile beyond the stability crossover size. In a supersaturated mother phase, the nucleation rate of a phase that is metastable in bulk form can sometime overcome that of a stable bulk phase

because of the lower surface free energy of the former.[14] Phase transitions to the stable phase occur subsequently.[15,16] In addition to rutile and anatase, an amorphous oxygen-deficient species columbite (α-PbO_2)-like phase and fluorite (CaF_2)-like cubic phase have been prepared as metastable forms through homogeneous nucleation of supersaturated titanium oxide vapor.[1,17–19] Although these studies successfully described the crystallographic characteristics of the nanoparticles in detail, the mechanism of the appearance and disappearance of metastable phases during nucleation remains unclear.

Homogeneous nucleation from supersaturated vapor is the key to understanding the formation of astronomical dusts around dying stars. The Universe is considered to be filled with solid-state particles produced by late-type giant stars, such as supernovae and asymptotic giant branch stars. The surface of the first solid to precipitate during dust formation provides heterogeneous reaction sites that trigger the formation of minerals and organic compounds around such stars.[20] Consequently, homogeneous nucleation of solid particles is a first step toward the formation of complex molecules in space. Thermodynamic calculations[21,22] suggest that titanium oxides are among the first condensates to form and that they operate as heterogeneous nucleation sites in dust formation.

We recently developed an in situ infrared observation system for studying the homogeneous nucleation of nanoparticles from highly supersaturated vapors.[23] To elucidate

66 the polymorphic appearance of titanium oxides in the homogeneous nucleation process, we
67 performed IR measurements in situ on nanoparticles nucleating from a highly supersaturated
68 vapor generated by the gas-evaporation method, an old-fashioned and simple technique for
69 the preparation of nanoparticles.[24] Features of the IR absorption band were also compared
70 with IR spectra of astronomical bodies to examine the possibility of whether titanium oxides
71 appear as an early condensate around evolved stars.
72
73 **2. Experimental Methods**
74 We performed nucleation experiments on titanium oxide nanoparticles, and we monitored
75 the process by using a Fourier transform IR (FT-IR) spectrometer (Spectrum 400;
76 PerkinElmer, Waltham, MA) with a triglycine sulfate (TGS) thermal detector, as described in
77 a previous study.[23] A schematic representation of the experiment is shown in Figure 1. The
78 height of the measurement points above the evaporation source can be changed from 2 cm for
79 newly nucleated particles to 6 cm for cooled nanoparticles. This permits the recording of
80 spectra of both newly nucleated and cooled nanoparticles. A series of experiments were
81 carried out independently under similar experimental conditions. The diameter of the IR beam
82 was 20 mm, so that the resulting IR spectra represented the average structure of nanoparticles
83 in a 20 mm **diameter** column.

The chamber was evacuated to a pressure below 1×10^{-4} Pa, the gate valve was closed, and high-purity O_2 (99.9%) and Ar (99.9999%) were injected. Initially, the pressure was raised to $(5.0 \pm 0.1) \times 10^2$ Pa with O_2 gas, and it was then raised to a total pressure of 1.0×10^4 Pa with Ar. The gas pressure was measured by means of a capacitance manometer (GM-1000, ULVAC Kiko Inc., Saito City). The evaporation source was a 30-mm-long tantalum wire with an optical axis $\phi = 1$ mm and a purity of 99.95% (Nilaco Corp., Tokyo), which was connected to Cu electrodes to permit rapid electrical-resistance heating. Temperature of the source was monitored by using a radiation thermometer ($\lambda = 0.8$–1.6 μm: FTZ2; Japan Sensor Corp., Tokyo). The emissivity of the tantalum metal was assumed to be fixed at 0.3 for the purposes of calculating the temperature. Titanium metal wire ($\phi = 0.1$ mm; purity: 99.9%) was coiled around the evaporation source. Gradual application of an AC voltage resulted in resistive heating of the evaporation source to 2200 ± 200 K within several seconds, at which stage the titanium metal wire evaporated. The resulting vapor flowed upward as a result of the thermal convection formed around the hot evaporation source and it subsequently cooled to induce homogeneous nucleation of nanoparticles, which were visible as a smoke. The resulting nanoparticles were collected on a stainless-steel sheet set 2 cm above the IR measurement points in each experiment.

The collected particles were picked up on a thin film of amorphous carbon mounted on a standard copper grid for transmission electron microscopy (TEM). The particles were then observed by TEM (JEM-2100F; JEOL Ltd., Tokyo) at an acceleration voltage of 200 kV. Particles from the collection holder were agitated with KBr powder, which was used to prepare pellets for subsequent FT-IR measurements.

3. Result and Discussion

Heating of the evaporation source to 2200 K resulted in the formation of white nanoparticles. IR spectra of the nucleating nanoparticle**s** recorded 2 cm from the source (Figure 2a) showed a broad band extending from 10 to 20 μm, which cannot be attributed to gas-phase molecules. Ti–O stretching and Ti–O–Ti bridging stretching modes appear in this region for sol–gel samples of titanium oxides (see, for example, Huang et al.[25]). Therefore, there is no doubt that the absorbing material in our experiments consisted of nascent nanoparticles of titanium oxides. The width of the band in this region is broader than that of the crystalline. We concluded that most of the titanium oxide nanoparticles nucleated as noncrystalline liquid droplets or in an amorphous solid form.

The spectrum recorded 6 cm from the source (Figure 2b) showed a sharper band centered at 12.8 μm. This peak is a diagnostic peaks for crystalline anatase, as calculated from the

optical constants of spherical particles.[26] This evolution of the IR spectra as the nanoparticles cooled showed that a phase transition occurred while they were free flying. The long-range ordered structure of TiO_6 octahedra shows a sharp absorption at about 13–14 μm. The newly nucleated titanium oxides nanoparticles did not show this absorption. Subsequent crystallization resulted in the formation of anatase.

Nucleation occurred exclusively from highly supersaturated vapors in our experimental gas-evaporation system. Recent in situ interferometric studies on the homogeneous nucleation of manganese metal and tungsten oxide showed that the critical nuclei consisted of 3 ± 1 atoms and 8 ± 1 molecules, respectively.[27,28] Molecular-dynamics simulations on Lenard–Jones molecules also showed that the critical nuclei in an atmosphere with a supersaturation ratio of more than 100 consist of about 10 atoms.[16,29–31] Because physical conditions such as the total pressure of the enclosed gas were the same as those in previous reports, the critical nuclei in this experiment were similarly expected to consist of a countable number of molecules; this is considerably smaller than the size for the crossover in stability from an amorphous phase to an anatase phases, which occurs at about 2 nm.[13] The IR spectrum shown in Figure 2 is the average image for a 20 mm diameter column. IR spectra are affected to a greater extent by larger nanoparticles because of their greater volume fraction. Size distributions of the products were therefore studied by TEM observations. Typical TEM

137 images and corresponding electron-diffraction patterns of the nanoparticles collected at 4 and
138 8 cm above the evaporation source are shown in Figure 3. Radius of a nanoparticle was
139 measured directly from TEM images and the average radii for 150 nanoparticles collected at 4
140 and 8 cm above the evaporation source were 27.5 ± 7.1 and 27.5 ± 6.3 nm, respectively. The
141 minimum and maximum radii observed were about 5 and 55 nm, respectively, in both samples.
142 Amplitude of absorbance arises from nanoparticles with relatively larger volume. The radii
143 corresponding to the average volumes calculated from the 150 nanoparticles represented in
144 the IR spectra were $31.4^{+7.6}_{-17.8}$ and $30.4^{+5.3}_{-8.3}$ nm for the nanoparticles collected at 4 cm and
145 at 8 cm, respectively. Newly nucleated nanoparticles grew to a size of the order of tens of
146 nanometers in diameter and the titanium oxide molecules were exhausted at rates that were
147 orders of magnitude faster than the typical convection velocity of the smoke (10 cm/s; see
148 Supplementary Information, Section 1). Under these types of conditions, nucleation always
149 occurs and most of the growth units are exhausted within a distance of a few millimeters from
150 the evaporation source.[27,28,32] The IR spectra shown in Figure 2a can therefore be considered
151 to represent newly nucleated nanoparticles with sizes of the order of several tens of
152 nanometers that had completed vapor growth. This showed that the transition from an
153 amorphous to a stable crystalline phase did not occur at the crossover size for the shift in
154 thermodynamic stability from amorphous titanium dioxide to anatase, which is about 2 nm.

155 Spherical nanoparticles of anatase were observed in both samples, which is consistent
156 with the results of IR spectroscopy. Nanoparticles collected at 4 cm are rapidly quenched by
157 attachment to the collecting sheet and their state is preserved. These particles showed
158 diffraction rings attributed to other crystalline structures and halo patterns caused by
159 amorphous particles. The diffraction spots can be explained by the present of titanium oxides
160 with an oxygen-deficient stoichiometry, such as Ti_8O_{15} (JCPDS card no.18-1404), Ti_9O_{17}
161 (JCPDS card no. 18-1405) or $Ti_{10}O_{19}$ (JCPDS card no. 11-474) which are known as Magnéli
162 phases. Though weak diffraction spots close to (101) in Figure 3b indicate that minute amount
163 of oxygen deficient titanium oxide were also contained, neither the other crystalline phases
164 nor amorphous were observed abundantly in the case of the nanoparticles collected at 8 cm.
165 An example of a high-resolution TEM micrograph of a Ti_8O_{15} crystalline nanoparticle and its
166 fast Furrier transform (FFT) image is shown in Figure 4.

167 These oxygen-deficient phases become thermodynamically stable when the O/Ti ratio is
168 near 1.8.[33] Furthermore, nonhomogeneous contrasts resulting from distortion and edge
169 dislocations were frequently observed for quenched nanoparticles. The formation of
170 oxygen-deficient crystalline phases of titanium oxides and the presence of greater numbers of
171 defects exclusively in the nanoparticles collected at 4 cm from the evaporation source suggest
172 that a portion of the noncrystalline nanoparticles had a O/Ti ratio of less than 2 during the

initial stages of crystallization. Subsequent crystallization involves gradual oxidation of the free-flying nanoparticles. The lattice fringes in Figure 4 disappeared at the surfaces of the particles. The appearance of an amorphous state at the surface of a particle with a crystalline interior is consistent with the results of molecular-dynamics simulations.[34] This suggests that secondary nucleation induces anatase formation through a homogeneous reaction in metastable noncrystalline particles.

The additional peak that appeared at 10.5 μm (Figure 2b) cannot be attributed to anatase or rutile. This unidentified band might derive from crystalline oxygen-deficient titanium oxides. No distinct IR spectra of Magnéli phases have been reported in any previous study because such phases are difficult to isolate.

The collected nanoparticles were embedded in a KBr medium and their IR spectra were recorded by means of the conventional pellet technique (Figure 5). A band at 10.5 μm was present in the spectrum of the sample collected 4 cm from the source (Figure 5a) and in that of free-flying particles (Figure 2b) but was absent in the spectrum of the sample collected 8 cm from the source (Figure 5b). This temporary appearance of the 10.5 μm band suggests that the nanoparticles were transformed into anatase while they were free flying. We propose that oxygen-deficient titanium oxides are formed in the nucleation process and that subsequent oxidation leads to their transformation into anatase.

191 The temperature field around the evaporation source under similar conditions has been
192 examined in a previous study, and the typical convection velocity of the smoke is known to be
193 10 cm/s in a 10^4 Pa atmosphere.[23] The temperature of a free-flying nanoparticle can be
194 regarded as identical to that of the gas because of the rapid heat transfer (see Supplementary
195 Information, Section 2). By comparing the measured area for FT-IR and the growth conditions,
196 we estimated that crystallization is complete within 0.1–1 s at 500–700 K. We calculated the
197 rate of nucleation of crystalline anatase J in an amorphous titanium dioxide nanoparticle as a
198 function of the temperature; details are given in the Supplemental Information, Section 3. We
199 then defined the timescale for homogeneous nucleation, τ_{homo}, of a particle with volume V as
200 follows;

$$\tau_{homo} = \frac{1}{J \times V}$$

201 We calculated τ_{homo} for a spherical particle with radius r = 50 nm, which we chose as an
202 upper boundary for this study (Figure 6). The evaluated waiting time for nucleation of anatase
203 from the amorphous phase had an order of magnitude in excess of 0.1–1 s over the entire
204 temperature range. The nucleation rate is sensitive to the activation energy E_a and to the
205 interfacial energy between anatase and the amorphous phase; we used a value of γ = 0.379 J
206 m^{-2} for the latter, as this is intermediate between that of anatase and liquid titanium dioxide.[35]
207 In general, nucleation rates for crystallization in a supercooled liquid droplet are higher **as**

208 a result of a reduction in activation energy (E_a/k), for example, from 38000 to 23000 K in the
209 case of silicate.[36–38] Unfortunately, the activation energy for crystallization of titanium oxides
210 in a supercooled liquid state has never been reported. Consequently, a quantitative comparison
211 of nucleation rates and crystallization velocities from the liquid phase and from the
212 amorphous phase cannot be presented here. If we assume that the activation energy for
213 crystallization from liquid droplets falls to 14000 K compared with the average value of
214 17400 K obtained experimentally for crystallization from the amorphous phase,[39–40] the
215 waiting time for nucleation approximates to the value determined in our experiment, shown
216 by dashed line in Figure 6. Molecular-dynamics simulations showed that the melting
217 temperature of titanium oxides falls markedly with increasing oxygen deficiency. For instance,
218 the melting temperature for titanium oxide falls by 33% when it has 12.5% of oxygen
219 vacancies, corresponding to a stoichiometry of Ti_4O_7.[41] Molecular-dynamics simulations of
220 titanium dioxide nanoparticles at various temperatures showed that the loss of the X-ray
221 diffraction peak that indicates melting occurs at lower temperatures than those measured for
222 the bulk material, e.g. <1200 K for 2 nm anatase spheres.[42] The reduction in the melting
223 temperature due to size effects and oxygen deficiency promotes the formation of liquid
224 droplets in the initial stages of nucleation. Rapid crystallization at a relatively low temperature
225 and the decrease in the melting temperature of oxygen-deficient titanium oxides suggest that

226 the noncrystalline particles are droplets of molten liquid.

227 Thermochemical calculations showed that crystallization of anatase from supercooled
228 liquid droplets occurs at T < 2057 K.[35] Because the temperature of a particle was much lower
229 than 2057 K in our experiments, the nucleation of anatase proceeded under high supercooling.

230 Nucleation of titanium oxides as liquid droplets has been directly measured, as in the case
231 of silicate.[23] Next, we will examine the generality of nucleation via liquid droplet, taking into
232 account the nucleation of liquid and crystalline phases from supersaturated vapor. In classical
233 nucleation theory, the change in the Gibbs free energy of a system on formation of nuclei of a
234 critical size from a supersaturated vapor is proportional to the ratio of the disadvantageous
235 effect of the surface and the advantageous effect of chemical-bond formation in the bulk
236 material ($\Delta G \propto \gamma^3/\Delta\mu^2$, where γ is the surface free energy and $\Delta\mu$ is the difference in
237 chemical potential compared with the vapor). In general, the surface free-energy value of the
238 crystalline phase is larger than that of the liquid (amorphous) phase ($\gamma_c > \gamma_l$). On the other
239 hand, the difference in chemical potential between the vapor and crystalline phases is always
240 larger than that between the vapor and liquid phases ($\Delta\mu_c > \Delta\mu_l$). When the supersaturation
241 ratio is smaller ($\Delta\mu_c \sim \Delta\mu_l$), the nucleation rate of the liquid overcomes that of the crystalline
242 form because of the lower surface free energy. In contrast, a crystalline nanoparticle tends to
243 nucleate directly from highly supersaturated vapor ($\Delta\mu_c > \Delta\mu_l$). Since the titanium oxide

244 nucleated as a liquid phase even in the present method, which makes very high
245 supersaturation ratio, reported metastable phases prepared by other physical process in which
246 supersaturation ratio at nucleation point may be smaller than or at least similar to our method,
247 such as laser ablation,[1,17–19] may also form via liquid droplets. Polymorphs branch off from
248 the liquid droplets in a manner that depends on their history after nucleation. We therefore
249 suggest that the O/Ti ratio of a particle and the cooling rate of the liquid droplets are the keys
250 to understanding the polymorphic behavior of titanium oxides. Figure 7 is a schematic
251 representation of the mechanism for the formation of anatase nanoparticles through
252 homogeneous nucleation of liquid droplets.

253 IR spectra of nanoparticles are the most important index for the observation of
254 astronomical dusts by telescopes. Fingerprints in the mid-IR region permit the identification
255 of minerals at great distances. In the laboratory, reference spectra are usually obtained after
256 embedding samples in highly transparent media. However, such spectra cannot readily be
257 compared with those of astronomical dusts because of the difference in the dielectric
258 constants of the surroundings between that of a vacuum ($\epsilon_m = 1$) and that of a dielectric
259 medium.[43] In our studies, the 12.8 μm peak of anatase shifted to 14.1 μm in KBr medium
260 (Figure 5b). The IR spectrum of anatase without an embedding effect has only been recorded
261 once previously; in that case, the peak for a commercial edged aggregate was centered at

13.10 μm.[44] The band width is also affected by the medium. The full width at half maximum of the band increased from 3.9 μm (Figure 2b) to 5.2 μm in KBr medium (Figure 5a). This is the first report of the appearance in IR spectra of a peak at 12.8 μm for spherical nanoparticles of anatase in the free-flying state ($\epsilon_m \sim 1$), which permits direct comparison with astronomical observations. A strong sharp feature has been detected at 13 μm around oxygen-rich evolved stars, and the carrier is often related to the first condensing mineral.[45,46] This 13 μm feature has not yet been successfully assigned. IR spectra of free-flying titanium oxides might assist in this assignment.

4. Conclusion

The nucleation of titanium oxides was studied by in situ IR measurement in the free-flying state. Newly nucleated nanoparticles showed broad noncrystalline features. Later, the cooled nanoparticles showed features of crystalline anatase. Therefore, titanium oxides nanoparticles nucleate in a metastable noncrystalline form that might consist of liquid droplets. Subsequent crystallization results in the formation of anatase. Identification of the nucleation in a noncrystalline phase provides general insight into the mechanism of formation of particles through homogeneous nucleation from the vapor phase. Free-flying particles and quenched product collected 4 cm from the evaporation source showed an unidentified band near

10.5 μm that disappeared in product collected at 8 cm. TEM observations revealed the presence of an oxygen-deficient crystalline form in product collected at 4 cm. The appearance of the peak at 10.5 μm appears to be connected with the formation of oxygen-deficient species. The appearance of oxygen-deficient species as an intermediate phase and the crystallization with oxidation of particles are both consistent with the obtained results. When IR spectra of collected product were measured by a conventional KBr pellet technique, the peak wavelength was shifted toward a longer wavelength and the band widths were broadened by the embedding effect of the dielectric medium. The 12.8 μm band of anatase identified here can be compared directly with astronomical observations. This could aid in the identification of the 13 μm band frequently observed for oxygen-rich evolved stars.

Associated Content

Details of estimations of the growth velocity of a nucleus in our experiment, of the time scale for a thermal equilibration between a free-flying nanoparticle and its surrounding atmosphere, and of the nucleation rate of crystals in a supercooled liquid droplet are available as supporting information.

Acknowledgements

This work was partly supported by a Grant-in-Aid for a JSPS Fellow (15J02433), a Grant-in-Aid for Scientific Research(S) from KAKENHI (15H05731), and the Japan–Slovenia Research Cooperative Program by JSPS and MIZS.

References

(1) Harano, A.; Shimada, K.; Okubo, T.; Sadakata, M. Crystal Phases of TiO_2 Ultrafine Particles Prepared by Laser Ablation of Solid Rods. *J. Nanopart. Res.* **2002**, *4*, 215–219.

(2) Atou, Y.; Suzuki, H.; Kimura, Y.; Sato, T.; Tanigaki, T.; Saito, Y.; Kaito, C. Novel Method for the Preparation of Silicon Oxide Layer on TiO_2 Particle and Dynamic Behavior of Silicon Oxide Layer on TiO_2 Particle. *Phys. E (Amsterdam, Neth.)* **2003**, *16*, 179–189.

(3) Matsubara, M.; Yamaki, T.; Itoh, H.; Abe, H.; Asai, K. Preparation of TiO_2 Nanoparticles by Pulsed Laser Ablation: Ambient Pressure Dependence of Crystallization. *Jpn. J. Appl. Phys.* **2003**, *42*, L479.

(4) McHale, J. M.; Auroux, A.; Perrotta, A. J.; Navrotsky, A. Surface Energies and Thermodynamic Phase Stability in Nanocrystalline Aluminas. *Science* **1997**, *277*, 788–791.

(5) Tavakoli, A. H.; Maram, P. S.; Widgeon, S. J.; Rufner, J.; van Benthem, K.; Ushakov, S.; Sen, S.; Navrotsky, A. Amorphous Alumina Nanoparticles: Structure, Surface Energy, and Thermodynamic Phase Stability. *J. Phys. Chem. C* **2013**, *117*, 17123–17130.

(6) Shandalov, M.; McIntyre, P. C. Size-Dependent Polymorphism in HfO_2 Nanotubes and Nanoscale Thin Films. *J. Appl. Phys.* **2009**, *106*, 084322.

(7) Garvie, R. C. Stabilization of the Tetragonal Structure in Zirconia Microcrystals. *J. Phys. Chem.* **1978**, *82*, 218–224.

(8) Chraska, T.; King, A. H.; Berndt, C. C. On the Size-Dependent Phase Transformation in Nanoparticulate Zirconia. *Mater. Sci. Eng., A* **2000**, *286*, 169–178.

(9) Zhang, Y. L.; Jin, X. J.; Rong, Y. H.; Hsu T. Y.; Jiang, D. Y.; Shi, J. L. The Size Dependence of Structural Stability in Nano-Sized ZrO_2 Particles. *Mater. Sci. Eng., A* **2006**, *438-440*, 399–402.

(10) Zhang, H.; Banfield, J. F. Understanding Polymorphic Phase Transformation Behavior During Growth of Nanocrystalline Aggregates : Insights from TiO_2. *J. Phys. Chem. B* **2000**, *104*, 3481–3487.

(11) Barnard, A. S.; Curtiss, L. A. Prediction of TiO_2 Nanoparticle Phase and Shape Transitions Controlled by Surface Chemistry. *Nano Lett.* **2005**, *5*, 1261–1266.

(12) Zhang, H., Banfield, J. F. Thermodynamic Analysis of Phase Stability of Nanocrystalline Titania. *J. Mater. Chem.* **1998**, *8*, 2073–2076.

(13) Zhang, H.; Chen, B.; Banfield, J. F.; Waychunas, G. A. Atomic Structure of Nanometer-Sized Amorphous TiO_2. *Phys. Rev. B: Condens. Matter Mater. Phys.* **2008**, *78*, 214106.

(14) Ostwald, W. Studien über die Bildung und Umwandlung Fester Körper. *Z. Phys. Chem.*, *Stoechiom. Verwandtschaftsl.* **1897**, *22*, 289–330.

(15) Stranski, I. N.; Totomanow, D. Rate of Formation of (Crystal) Nuclei and the Ostwald Step Rule. *Z. Phys Chem., Abt. A* **1933**, *163*, 399–408.

(16) Tanaka, K. K.; Tanaka, H.; Yamamoto, T.; Kawamura, K. Molecular Dynamics Simulations of Nucleation from Vapor to Solid Composed of Lennard–Jones Molecules. *J. Chem. Phys.* **2011**, *134*, 204313.

(17) Hirasawa, M.; Seto, T.; Orii, T.; Aya, N.; Shimura, H. Synthesis of Size-Selected TiO_x Nanoparticles. *Appl. Surf. Sci.* **2002**, *198*, 661–665.

(18) Chen, S. Y.; Shen, P. Laser Ablation Condensation of α-PbO_2-Type TiO_2. *Phys. Rev. Lett.* **2002**, *89*, 096106.

(19) Tsai, M. H.; Shen, P.; Chen, S. Y. Defect Generation of Anatase Nanocondensates via Coalescence and Transformation from Dense Fluorite-Type TiO_2. *J. Appl. Phys.* **2006**,

100, 114313.

(20) Tielens, A. G. G. M. *The Physics and Chemistry of the Interstellar Medium*; Cambridge University Press: Cambridge, U.K., **2005**.

(21) Gail, H.-P.; Sedlmayr, E. Inorganic Dust Formation in Astrophysical Environments. *Faraday Discuss.* **1998**, *109*, 303–319.

(22) Goumans, T. P. M.; Bromley, S. T. Stardust Silicate Nucleation Kick-Started by SiO + TiO_2. *Philos. Trans. R. Soc., A* **2013**, *371*, 20110580.

(23) Ishizuka, S.; Kimura, Y.; Sakon, I. In Situ Infrared Measurements of Free-Flying Silicate During Condensation in the Laboratory. *Astrophys. J.* **2015**, *803*, 88.

(24) *Ultra-Fine Particles: Exploratory Science and Technology*; Hayashi, C.; Uyeda, T.; Tasaki, A., Eds.; Noyes Publications: Westwood, N. J., **1997**.

(25) Huang, D.; Liao, S.; Quan, S.; Liu, L.; He, Z.; Wan, J.; Zhou, W. Preparation of Anatase F Doped TiO_2 Sol and Its Performance for Photodegradation of Formaldehyde. *J. Mater. Sci.* **2007**, *42*, 8193–8202.

(26) Posch, T.; Kerschbaum, F.; Fabian, D.; Mutschke, H.; Dorschner, J.; Tamanai, A. Infrared Properties of Solid Titanium Oxides: Exploring Potential Primary Dust Condensates. *Astrophys. J. Suppl. Ser.* **2003**, *149*, 437–445.

(27) Kimura, Y.; Tanaka, K. K.; Miura, H.; Tsukamoto, K. Direct Observation of the

Homogeneous Nucleation of Manganese in the Vapor Phase and Determination of Surface Free Energy and Sticking Coefficient. *Cryst. Growth Des.* **2012**, *12*, 3278–3284.

(28) Kimura, Y.; Miura, H.; Tsukamoto, K.; Li, C.; Maki, T. Interferometric In-Situ Observation during Nucleation and Growth of WO_3 Nanocrystals in Vapor Phase. *J. Cryst. Growth* **2011**, *316*, 196–200.

(29) Diemand, J.; Angélil, R.; Tanaka, K. K.; Tanaka, H. Large Scale Molecular Dynamics Simulations of Homogeneous Nucleation. *J. Chem. Phys.* **2013**, *139*, 074309.

(30) Angélil, R.; Diemand, J.; Tanaka, K. K.; Tanaka, H. Properties of Liquid Clusters in Large-Scale Molecular Dynamics Nucleation Simulations. *J. Chem. Phys.* **2014**, *140*, 074303.

(31) Tanaka, K. K.; Diemand, J.; Angélil, R.; Tanaka, H. Free Energy of Cluster Formation and a New Scaling Relation for the Nucleation Rate. *J. Chem. Phys.* **2014**, *140*, 194310.

(32) Kimura, Y.; Tsukamoto, K. Interferometric Observation of Temperature Distributions in the Smoke Experiment. *J. Jpn. Microgravity Appl.* **2011**, *28*, S9–S12.

(33) Roy, R.; White, W. B. Growth of Titanium Oxide Crystals of Controlled Stoichiometry and Order. *J. Cryst. Growth* **1972**, *13–14*, 78–83.

(34) Banfield, J. F.; Zhang, H. Nanoparticles in the Environment. *Rev. Mineral. Geochem.* *44*, 1–58.

(35) Li, Y.; Ishigaki, T. Thermodynamic Analysis of Nucleation of Anatase and Rutile from TiO_2 Melt. *J. Cryst. Growth* **2002**, *242*, 511–516.

(36) Nagashima, K.; Tsukamoto, K.; Satoh, H.; Kobatake, H.; Dold, P. Reproduction of Chondrules from Levitated, Hypercooled Melts. *J. Cryst. Growth* **2006**, *293*, 193–197.

(37) Tanaka, K. K.; Yamamoto, T.; Nagashima, K.; Tsukamoto, K. A New Method of Evaluation of Melt/Crystal Interfacial Energy and Activation Energy of Diffusion. *J. Cryst. Growth* **2008**, *310*, 1281–1286.

(38) Tanaka, K. K.; Yamamoto, T.; Kimura, H. Low-Temperature Crystallization of Amorphous Silicate in Astrophysical Environments. *Astrophys. J.* **2010**, *717*, 586–596.

(39) Howitt, D. G. The Oriented Growth of Anatase in Thin Films of Amorphous Titania. *J. Mater. Res.* **1987**, *2*, 201–210.

(40) Exarhos, G. J.; Aloi, M. Crystalline Growth Kinetics in Isothermally Annealed Sol–Gel Films. *Thin Solid Films* **1990**, *193*, 42–50.

(41) Zhang, H.; Banfield, J. F. Kinetics of Crystallization and Crystal Growth of Nanocrystalline Anatase in Nanometer-Sized Amorphous Titania. *Chem. Mater.* **2002**, *14*, 4145–4154.

(42) Knaup, J. M.; Marx, J.; Frauenheim, T. Reduction of the TiO_{2-x} Melting Temperature Induced by Oxygen Deficiency with Implications on Experimental Data Accuracy and Structural Transition Processes. *Phys. Status Solidi RRL* **2014**, *8*, 549–553.

(43) Naicker, P. K.; Cummings, P. T.; Zhang, H.; Banfield, J. F. Characterization of Titanium Dioxide Nanoparticles Using Molecular Dynamics Simulations. *J. Phys. Chem. B* **2005**, *109*, 15243–15249.

(44) Bohren, C. F.; Huffman, D. R. *Absorption and Scattering of Light by Small Particles*; Wiley: New York, 1983.

(45) Tamanai, A.; Mutschke, H.; Blum, J.; Posch, T.; Koike, C.; Ferguson, J. W. Morphological Effects on IR Band Profiles: Experimental Spectroscopic Analysis with Application to Observed Spectra of Oxygen-Rich AGB Stars. *Astron. Astrophys.* **2009**, *501*, 251–267.

(46) Speck, A. K.; Barlow, M. J.; Sylvester, R. J.; Hofmeister, A. M. Dust Features in the 10-μM Infrared Spectra of Oxygen-Rich Evolved Stars. *Astron. Astrophys., Supp. Ser.*, **2000**, *464*, 437–464.

(47) Sloan, G. C.; Kraemer, K. E.; Goebel, J. H.; Price, S. D. Guilt by Association: The 13 Micron Dust Emission Feature and Its Correlation to Other Gas and Dust Features. *Astrophys. J.* **2003**, *594*, 483–495.

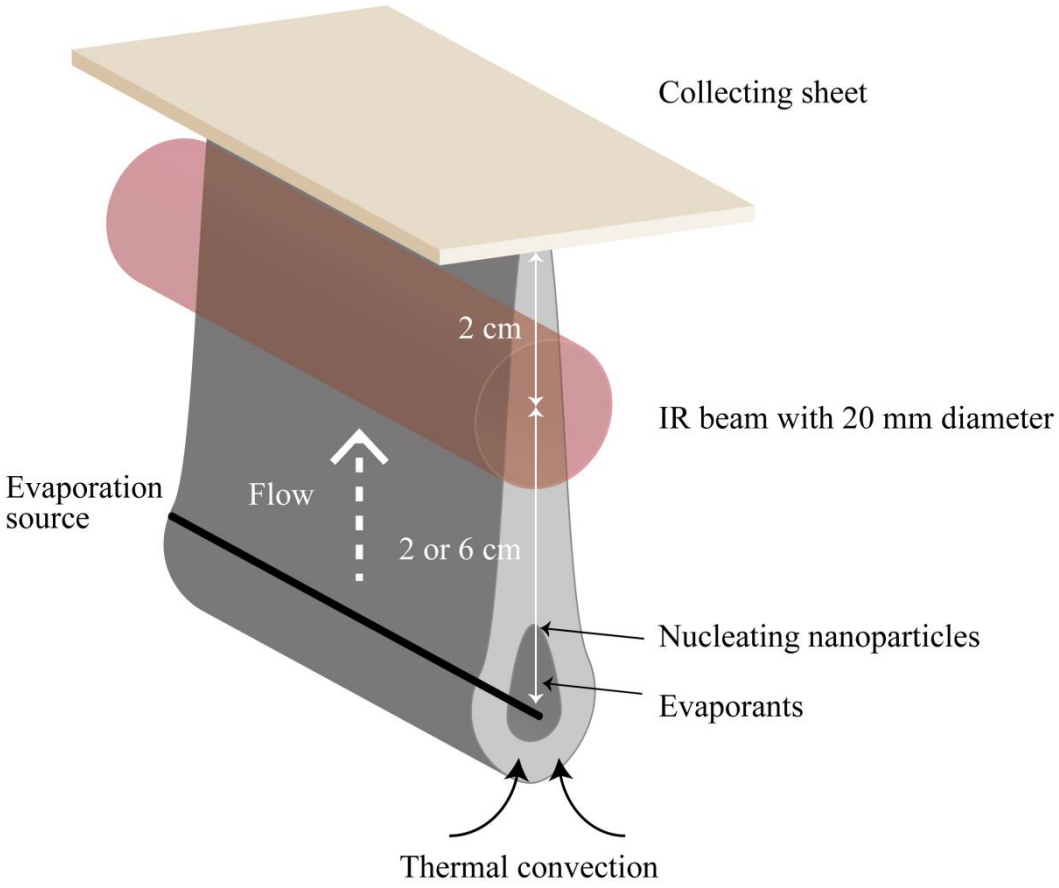

424

425 Figure 1. Schematic image of the experiment. Nanoparticles nucleate around the evaporation
426 source, cool in the flow by thermal convection and, then, can be seen as a smoke. IR spectra
427 of newly formed (2 cm above the evaporation source) and cooled (6 cm above the evaporation
428 source) nanoparticles are measured respectively. Some portion of the flowed nanoparticles
429 attaches to a collecting sheet set 2 cm above the IR beam.

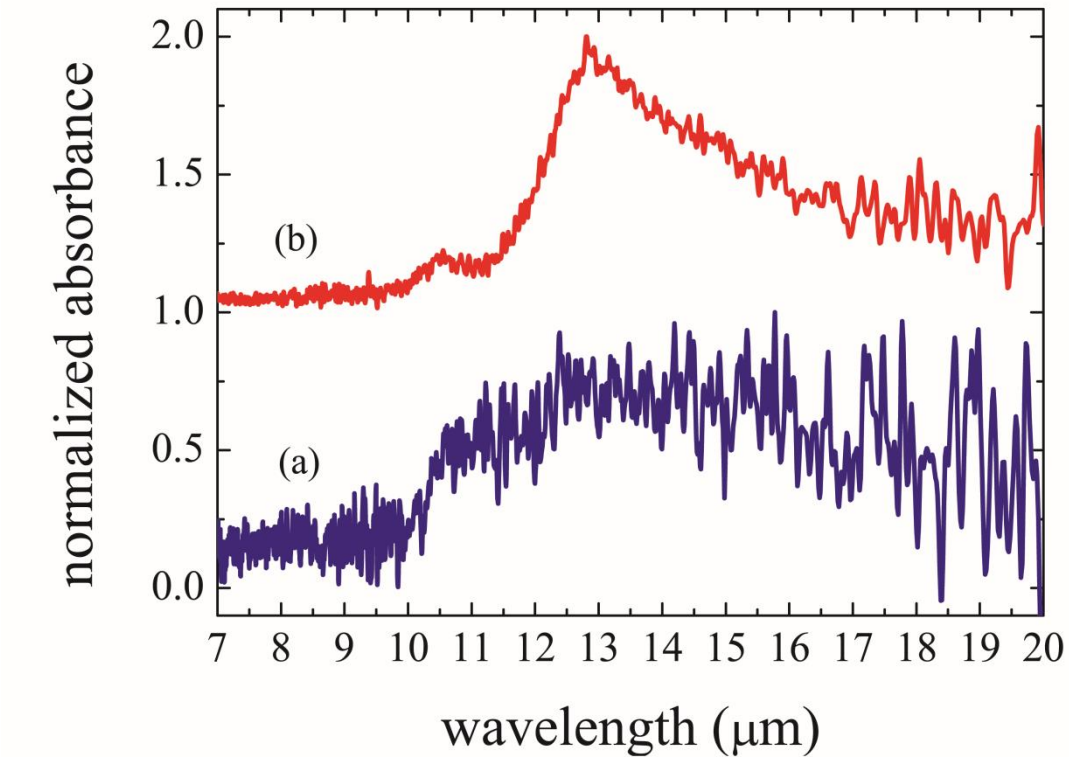

Figure 2. IR spectra of condensing titanium oxide nanoparticles measured (a) at 2 cm and (b) at 6 cm above the evaporation source.

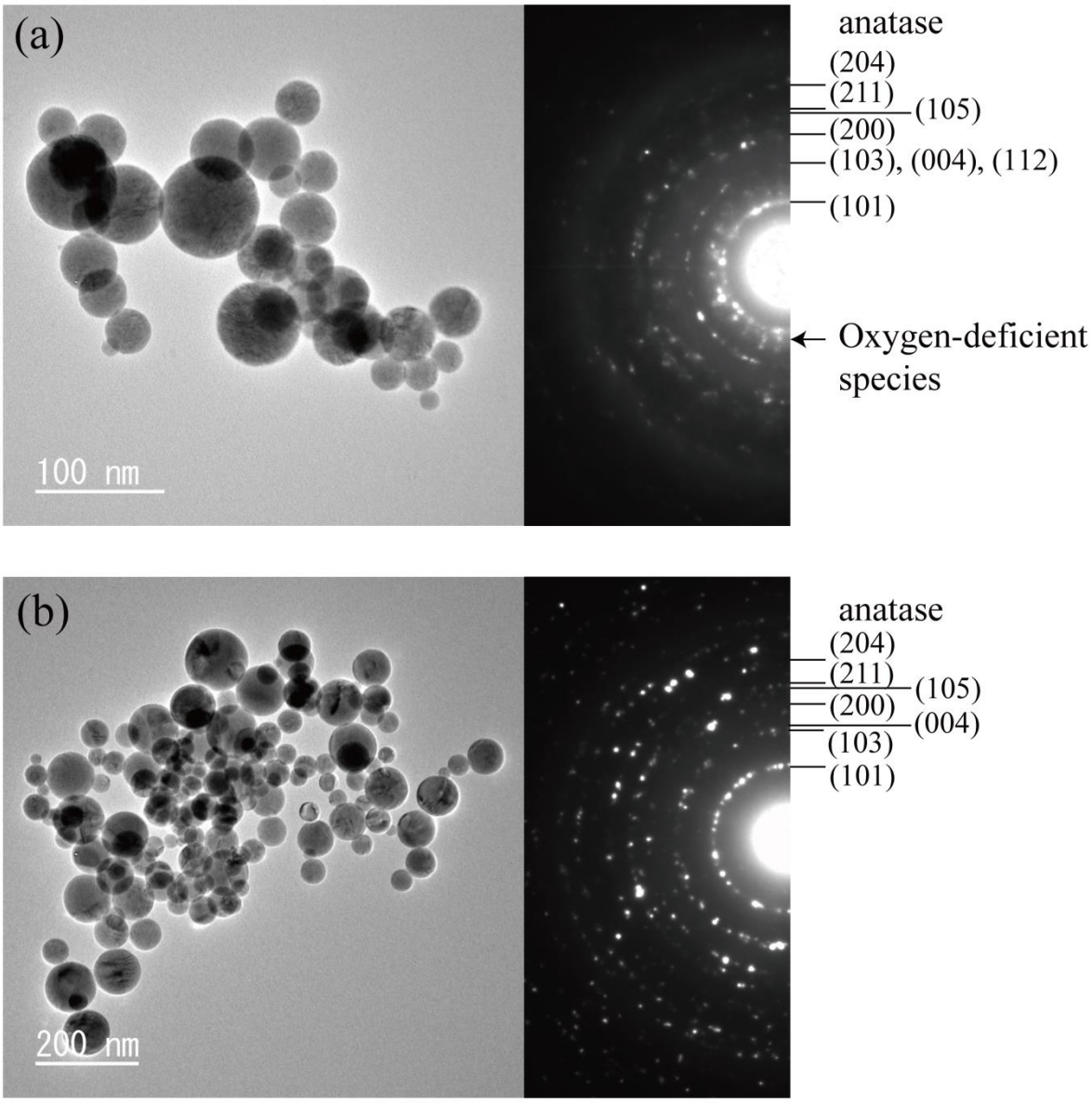

Figure 3. Bright-field TEM images and the corresponding electron-diffraction patterns of nanoparticles collected (a) at 4 cm and (b) at 8 cm above the evaporation source. Anatase (JCPDS card no. 21-1272) was the main product in both samples. A halo pattern caused by amorphous materials and diffraction rings attributed to oxygen-deficient titanium oxides were identified in the products collected at 4 cm.

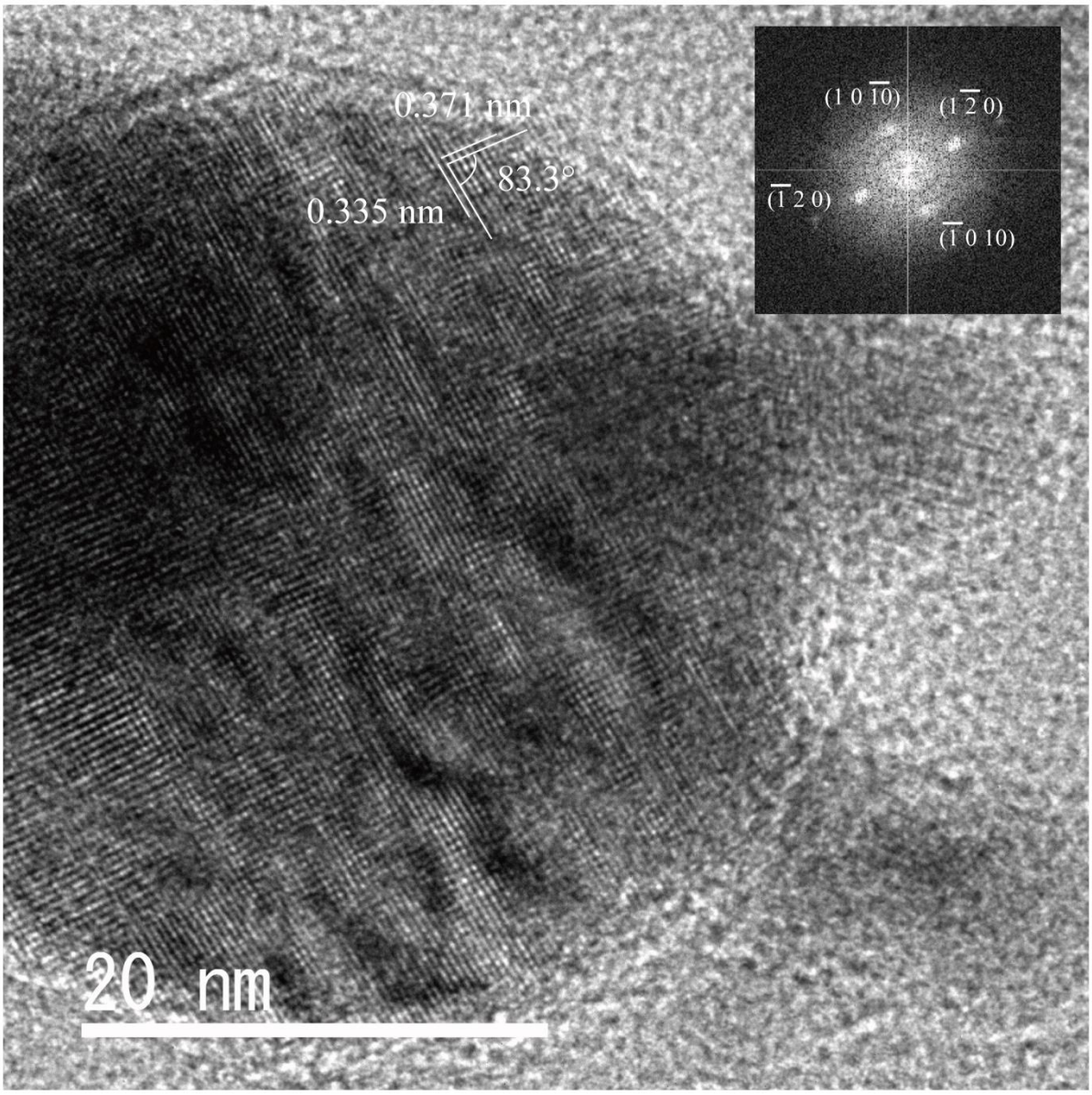

Figure 4. High-resolution TEM image of a nanoparticle collected 4 cm above the evaporation source and FFT analysis of the nanoparticle. Lattice fringes of 0.371 nm $(10\bar{1}0)$ and 0.335 nm $(1\bar{2}0)$ with a crossing angle at 83.3° indicate the formation of a nanoparticle of crystalline Ti_8O_{15}. Amorphous titanium oxide appears on the surface.

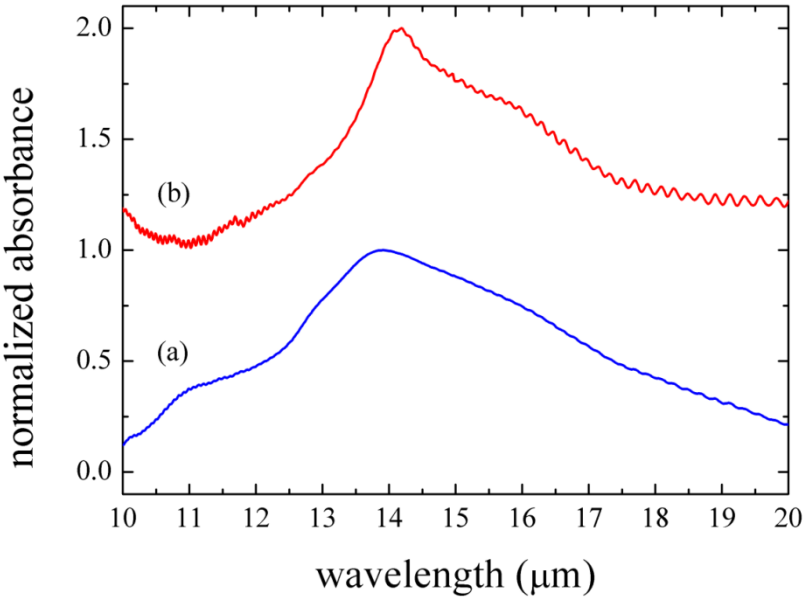

Figure 5. IR spectra recorded by the conventional KBr pellet technique of nanoparticles collected (a) at 4 cm and (b) at 8 cm above the evaporation source. The shapes of the spectra differ from those of the free-flying nanoparticles (Figure 2) due to effects of the medium. High frequency oscillation with small amplitude in the spectra is artificial fringes caused by internal reflection of a KBr pellet.

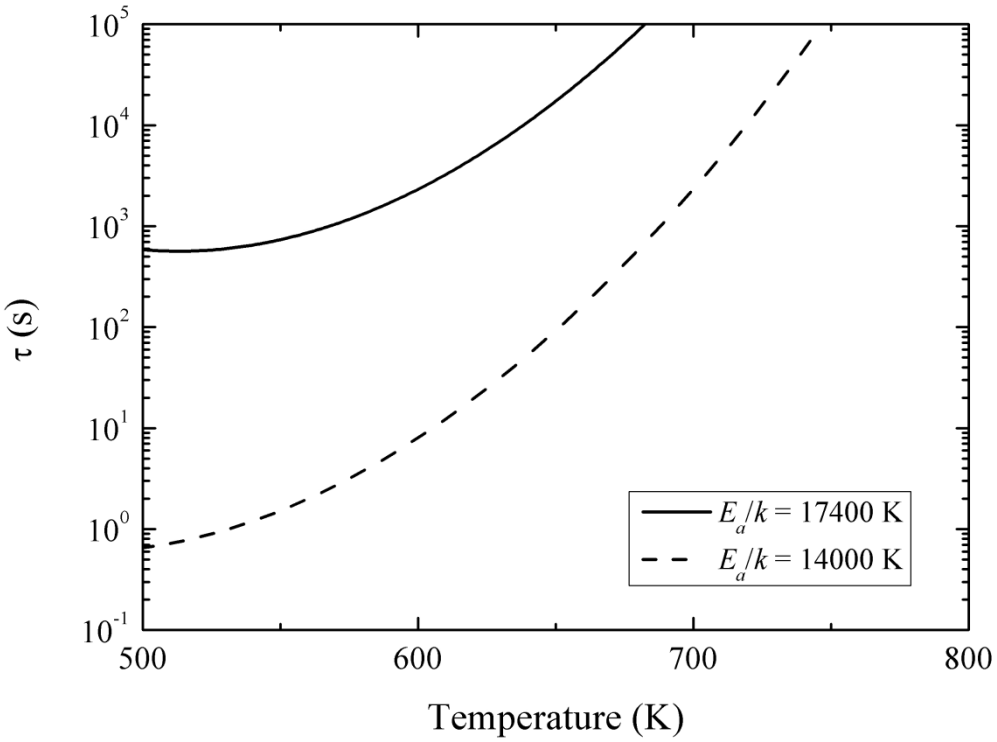

Figure 6. Time scales for homogeneous nucleation evaluated at the activation energy for crystallization from the amorphous phase of E_a/k = 17400 K (solid line) and the assumed value for crystallization from the liquid phase of E_a/k = 14000 K (dashed line), respectively.

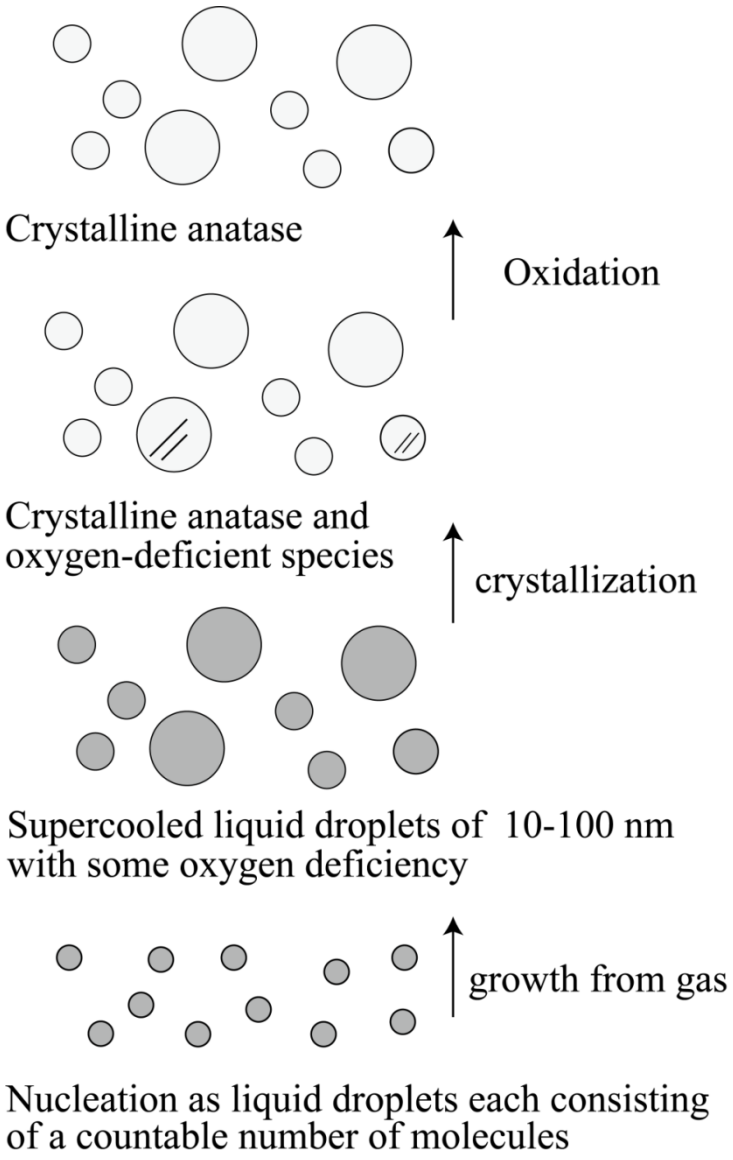

454

455 Figure 7. Mechanism of the formation of anatase nanoparticles through homogeneous

456 nucleation of liquid droplets from highly supersaturated vapor.